ELSEVIER

Thermochimica Acta 364 (2000) 11–22

thermochimica acta

www.elsevier.com/locate/tca

A modulated adiabatic scanning calorimeter (MASC)

G. Salvetti, C. Cardelli, C. Ferrari, E. Tombari*

IFAM/CNR, Area della Ricerca San Cataldo, via Alfieri 1, 56010 Ghezzano, Pisa, Italy

Received 16 May 2000; received in revised form 14 August 2000; accepted 20 August 2000

Abstract

The modulated adiabatic scanning calorimeter (MASC) described here is designed to work in both the time-domain (adiabatic-like step-scanning) and in the frequency domain (modulated temperature/power-scanning) operational modes. The cylindrical form of the cell and the controlled thermal environment in which the sample is located make it possible: (i) to write detailed and reliable equations to describe the heat flow; (ii) to derive analytical relations to calculate the energy release from the sample and the real and imaginary parts of the complex heat capacity at the modulation frequency; (iii) to study narrow phase transitions using the power modulated scanning mode; and (iv) to generate adiabatic-like conditions. The thermal environment is controlled by means of an active thermal shield which is kept at a temperature close to that of the sample cell in order to minimise the thermal gradients to which the sample is exposed. The temperature difference between the shield and the cell is set at the value required to control or cancel heat leakage from the cell. MASC can be used to carry out measurements on a single sample in different operational modes that can be made operative under the control of its built-in software. The parameters of interest can be automatically calculated by means of a program based on a model of the cell + sample system that will be described in a second paper.

To test the performance of the calorimeter, samples of materials which undergo a first-order phase transition or a glass transition (indium, ice, and polystyrene) were studied. The specific features of the calorimetric cell, the calibration procedure, and the experimental results are reported and discussed.

Keywords: Modulated adiabatic scanning calorimeter; Time-domain; Frequency-domain; Milling; Glass transition

1. Introduction

Calorimetry is an experimental technique that is widely used in many research fields, particularly in the material sciences, to study chemical, physical and biological processes. Ideally the calorimetric study of an unknown sample would make use of a ''first look'' run, obtained by scanning the temperature in the interval of interest. Based on this preliminary data, the most suitable mode for further calorimetric studies would be determined and applied. Many different operational modes have been developed, each one generally being recommended for certain applications and not others [1–3]. Unfortunately, all of the calorimeters currently available perform optimally in only a single mode, so more than one calorimeter (not all of which are commercially available) would be needed to carry out thorough studies. Thus, the ideal approach outlined above is not feasible for practical and economic reasons, and compromises are necessary. As a consequence, reliable and detailed calorimetric studies can be performed only on a limited class of samples and processes, unless the researchers have

* Corresponding author. Tel.: +39-50-3152536; fax: +39-50-3152230.
E-mail address: tombari@ifam.pi.cnr.it (E. Tombari).

0040-6031/00/$ – see front matter
PII: S0040-6031(00)00645-6

the resources to design and build the exact calorimeter for their needs in-house.

MASC, the calorimeter described here, is the most recent in a family of instruments developed in the authors' laboratory [4,5]. It offers a relatively simple and very flexible tool for solving problems of interest in many fields, where calorimetry can be usefully applied. The cylindrical symmetry of the sample cell and the control of its thermal environment provide the basis for a theoretical model which allows to derive the relationships between the measured quantities and the parameters that characterise the sample [5,6]. These features of MASC also make it possible to obtain all of the advantages of modulated temperature calorimetry (MTC), and can help expanding the field of frequency domain calorimetry [7,8]. At present MTC can be used with confidence only if the experimental conditions and the instrumental parameters are under control and do not vary with time [9–11].

The active thermal shield built into the MASC allows the user to control the heat flow to and from the sample in a highly accurate and reproducible manner during the experimental run. When the longitudinal heat losses of the cell are compensated for by the radial heat flow from the shield, an adiabatic-like operational mode is obtained.

MASC functions by controlling either the cell temperature itself or the power supplied to the cell. The quantity measured is therefore either the cell temperature as it changes up or down as a function of a programmed heat flow or the power supplied to the cell to track the programmed temperature profile. The stability over time and the reproducibility of the data makes the performance of this instrument comparable to that of twin-cell differential instruments.

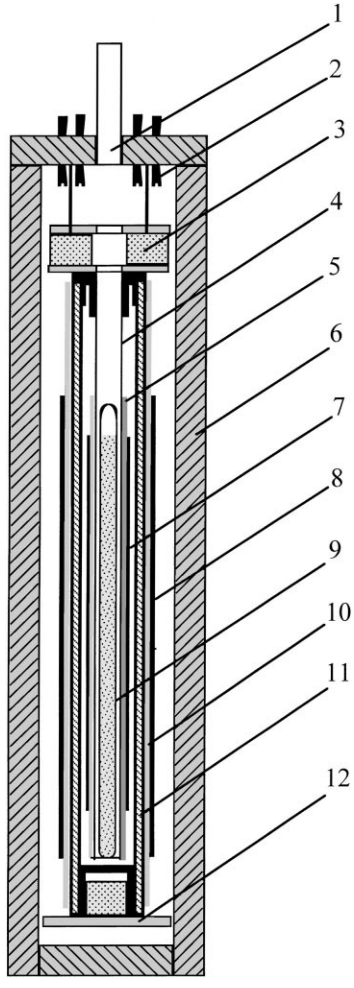

Fig. 1. Schematic and enlarged diagram showing a vertical section of the calorimetric head: 1, stainless steel tube for sample top-loading; 2, electrical links; 3, thermal insulator; 4, sample cell (stainless-steel); 5, cell heater (coated manganine wire); 6, thermal bath (aluminium); 7, cell temperature sensor (nickel alloy-99 type by Driver Harris); 8, shield temperature sensor (nickel alloy-99 type by Driver Harris); 9, sample container (pyrex); 10, thermal shield heater (coated manganine wire); 11, thermal shield (aluminium); 12, thermal insulator.

2. The instrument design and measuring procedures

The main features of the MASC, together with details of the cell design and the calibration procedure, are reported and discussed below.

2.1. The calorimetric head

The calorimetric head and the sample cell are shown schematically in Fig. 1. The novel feature of the MASC is its active thermal shield, which was introduced both to minimise the temperature gradient, ΔT, along the sample and to scan up and down the sample temperature by reproducible heat flows. Without this shield in the calorimeter, ΔT increases more and more markedly as the cell temperature, T, is scanned above the bath temperature, T_b (e.g. if $T > T_b + 100^\circ C$, ΔT was $1^\circ C$ as may be seen from

the apparent melting interval of an 8 cm sample of indium).

The instrument's program maintains T_b at a constant ($\pm 0.002^{\circ}C$) and suitable value ($\sim 20^{\circ}C$ below the starting point of the temperature interval being measured) and the shield temperature (T_s) at a distance δT above or below the cell temperature. During the experimental run the cell temperature may either: (i) change spontaneously; or (ii) follow a programmed temperature curve, as a function of the heat supplied to the cell and/or the heat flow from the shield. To achieve this, a pair of wires, one for the sensor and one for the heater, are wound uniformly around the outside of both the cell and the shield (Fig. 1). The cell sensor (nickel alloy 99 type, Driver Harris) measures the average temperature of the cell, which is practically equivalent to the sample temperature since the gradient along the cell length is very small (<10 mK) and the radial heat diffusion time in the cell + sample is <1 s if the temperature range of the experiment is far enough from the sample phase transition interval. The heaters of the MASC consist of metal resistors with a low temperature coefficient (coated manganine alloy).

A block diagram of the MASC with its principle components is shown in Fig. 2. The multimeters used to measure the sensor resistance and the applied voltage are commercially available instruments interfaced to a PC and controlled by a program written using LabVIEW software. The sensitivity of the instrument for temperature measurements is 0.1 mK.

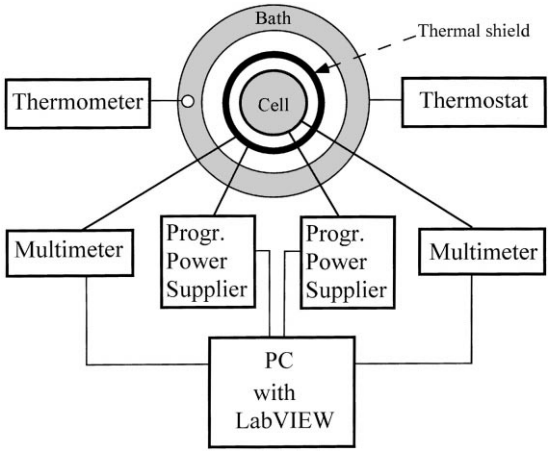

Fig. 2. Block diagram of the calorimeter.

The measured data are stored for the analysis and utilised in the control program during the experimental run. Two temperature control procedures, proportional-integral-differential (PID), are contained in the program: the first changes the cell temperature, T; while the second maintains $T - T_s = \delta T$. By changing the sign and value of δT it is possible to scan up and down the sample temperature. The same principle was utilised by Jeong in his modified adiabatic calorimeter [12].

The adiabatic-like conditions (power loss from the cell controlled to within $\pm 30\ \mu W$) created by the MASC can be used to study slow-rate exo/endothermic processes and to accurately measure transition enthalpies and temperatures. Thus the instrument is suitable for sample purity tests based on the melting-point depression [13].

2.2. The calibration procedure

The temperature calibration procedure involves two distinct phases. In the first phase the bath temperature, T_b, is gradually changed, covering the entire temperature interval (typically from 250 to 470 K) in incremental steps of a few degrees; no power is supplied to the cell or to the shield heaters. After each incremental step, and until equilibrium is attained, the resistance values, $R_i(t)$, for the heaters and sensors, and $T_b(t)$ are measured and automatically stored. A secondary, standard thermometer (Hart Scientific, mod. 501) measures T_b to an accuracy of $\pm 0.01^{\circ}C$, and the sample cell and the thermal shield temperatures are assumed to be equal to T_b. The plateaux of the experimental curves $R_i(t)$ and $T_b(t)$ are then fitted to calculate the R_i and T_b values. The sensor R_i against T curves are fitted to polynomial equations in order to obtain $T_i = f(R_i)$, the thermometric functions utilised in the MASC control program.

In the second phase, the accuracy of the MASC temperature scale is substantially improved by directly measuring the cell temperature. To do this the melting temperature of indium, water, and/or some other reference substance, with a transition interval width compatible with the accuracy to be attained, is first studied with MASC operating in the adiabatic-like mode. The temperature scale correction, generally a few hundredths of a degree at higher temperatures, is the difference between the tabulated reference

temperature and the value measured by the cell sensor according to the first phase of the calibration procedure.

During the course of an experimental run, the bath temperature is kept constant while the shield and cell temperatures are changed by supplying power to the heaters. When the shield temperature is increased to above the bath temperature, a temperature gradient occurs along the shield. This gradient results in a T_s value (i.e. the mean temperature value along the shield length covered by the sensor) that is lower than the temperature of that part of the shield which faces the cell. To minimise this effect, the length of the shield sensor is as long as the sample cell (Fig. 1). In any case, when no power is supplied to the cell, a temperature difference $\delta T(T) = T - T_s$ between the cell and the shield is present and its value increases more and more with the increasing difference between T_s and the bath temperature. $\delta T(T)$ can be accurately determined by step-scanning T_s with T_b kept constant and measuring the equilibrium T value. The measured $\delta T(T)$ values can be fitted to a second order polynomial equation (for example, when T_b is set at -25°C, one obtains $\delta T(T) = -0.1001 + 6.464 \times 10^{-3}\, T + 7.772 \times 10^{-6}\, T^2$).

During an experimental run T can change, either spontaneously or when power is supplied to the heaters, owing to exothermic processes occurring in the sample. If the shield temperature is maintained at $T - \delta T(T)$, the heat flow from the cell is null and adiabatic-like conditions are obtained.

The total heat flow to the cell can be maintained at a fixed value, Φ, by setting the shield temperature at the appropriate value $T_s = T - \delta T(T) + \Phi/\lambda(T)$, where $\lambda(T)$ is the heat exchange coefficient between the shield and the cell. At room pressure the temperature dependence of the heat exchange coefficient is: $\lambda(T) = 26.6 \times 10^{-3} + 8.73 \times 10^{-5}\, T + 6.48 \times 10^{-8}\, T^2$.

The experimental criterion for the attainment of adiabatic-like conditions is the stability of $T(t)$ for a time longer than the measurement interval. This means that during this interval longitudinal heat losses are balanced by the radial heat flow. This is always possible, but a temperature gradient along the sample is the inescapable price to be paid. To minimise this effect in the MASC, particular attention was devoted to the thermal insulation of the cell top, which is open for sample loading. A simple and reliable way to test the temperature gradient along the cell is to study the sharp phase transition of indium. We found that an indium sample filling 90% of the cell length (Fig. 1) apparently melts along a temperature interval that is as large as the temperature gradient along the cell itself, the melting interval of indium being only 0.0012 K (see experimental results reported below).

The power supplied to the MASC cell is calculated from the known heater resistance, which is invariant over time, and the applied voltage value measured using a multimeter (Keithley, mod. 2010). The resulting accuracy is sufficient for most purposes. To increase the accuracy of the power measurement, so that it is higher than the sensitivity of the calorimeter, a four-wire connection to the cell heater for the simultaneous measurement of current and voltage can be used.

3. MASC operation modes

The MASC operational modes are listed in Table 1. When working in modes A, B or C, the power supplied to the cell heater is the measured quantity.

The shield temperature is generally set below the cell temperature in order to maintain a fixed negative heat flow. Under these conditions the cell temperature can be scanned up and down by manipulating the power supplied to the cell heater. In the other modes the thermal shield is utilised to supply controlled heat flows to the sample cell or to compensate for the longitudinal heat losses so as to obtain adiabatic-like conditions. In these modes the cell temperature is the quantity measured during the experimental run.

The cell temperature can be assumed to be equal to the sample temperature only at equilibrium. This condition is attained after just a few seconds if the cell is filled with a sample that is far from its phase transitions, as the characteristic time of the radial heat flow is less than 1 s. In contrast, the spatial uniformity of the sample temperature cannot be attained in a short period of time within the phase transition interval. The measured $P(t)$ or $T(t)$ describe the heat storage process in the cell + sample system and generally relaxes toward the equilibrium value with a characteristic time. In principle the relaxation time contains information both on the heat diffusion within the non-homogeneous sample and on the heat absorption/

Table 1
MASC operational modes and their potential fields of application

Calorimetric modes	Measured quantity	Derived quantities	Features and application fields
(A) *T*-scan	$P(t)$	ΔH, C_p	First-look runs and fast measurements
(B) *T*-step scan	$P(t)$	ΔH, C_p, τ	Time domain High sensitivity Phase transitions
(C) *T*-modulation added to (A) and (B)	$P(\omega)$	$C_p * (\omega)$	Frequency domain Separation of *T*-dependent from *T*-independent processes
(D) Enthalpy-scan (at constant power)	$T(t)$	ΔH, C_p	Fast runs as in mode (A) Phase-transitions
(E) Enthalpy-step scan	T(t)	C_p, ΔH, τ, T_{eq}	Time domain Phase transitions
(F) *P*-modulation added to (D) and (E)	$T(\omega)$	$C_p * (\omega)$	The features of mode (C) Very sharp transitions

release rate, i.e. on the phase transition process. In this case the analysis is not straightforward as the cell temperature represents the mean temperature of the sample only when the total heat flow from the cell surface is null. Consequently the temperature measured on the cell during a scanning and/or modulated run is not coincident with the sample temperature. G.W.H. Höhne recently presented a ''low pass filter'' model designed to correct the heat capacity and temperature of a sample measured by modulated calorimetry [9]. The ''real'' sample properties can be measured only if the temperature relaxation time, τ of the cell + sample system is known. MASC can calculate τ from an analysis of the time-domain data obtained using the adiabatic-like step-scanning mode, so that modulated calorimetry can also be applied to the study of the phase transition region using Höhne's model.

4. Examples of the application of MASC

The first-order phase transitions of indium and water and the glass transition of a thermoplastic polymer were studied to demonstrate the main features of MASC's operational modes and the advantages of their combined use on a single sample. Moreover, the features of the melting of indium and of water were used to calibrate the MASC time scale within the phase transition interval and to develop a model of the cell + sample system [6].

4.1. Indium melting

The melting of 0.3647 g of indium (purity 99.999%, Aldrich), as observed in the temperature scanning mode at a rate of 1 K/h, is shown in Fig. 3. A linear increase in the measured power against temperature is present on the low temperature side of the melting peak. Small deviations occur only at the beginning and near the maximum. Conventional DSC analysis [14] places the melting onset at 156.63°C.

An adiabatic-like step-scanning run, performed with heat pulses of 0.25 J, supplied at intervals of 900 s for a period 25 s, is shown in Fig. 4. The melting temperature, as derived from the ''plateau'' of the *T* against time curve, is 156.626°C. The ''plateau'' actually exhibits a width, i.e. the melting occurs in an temperature interval of 0.0012°C. The temperature profiles following each heat pulse (see insert, Fig. 4) are well fitted, if one discards the first two points (4 s), by a single exponential decay function. The relaxation time, τ, against the supplied heat, Q, together with the melting curves measured using different calorimetric operational modes, are shown in Fig. 5. The *Q*-scan curve is obtained by supplying 5 mW to the cell under adiabatic-like conditions. The *T*-scan curve is calculated by the integration of $P(t)$, the power supplied to

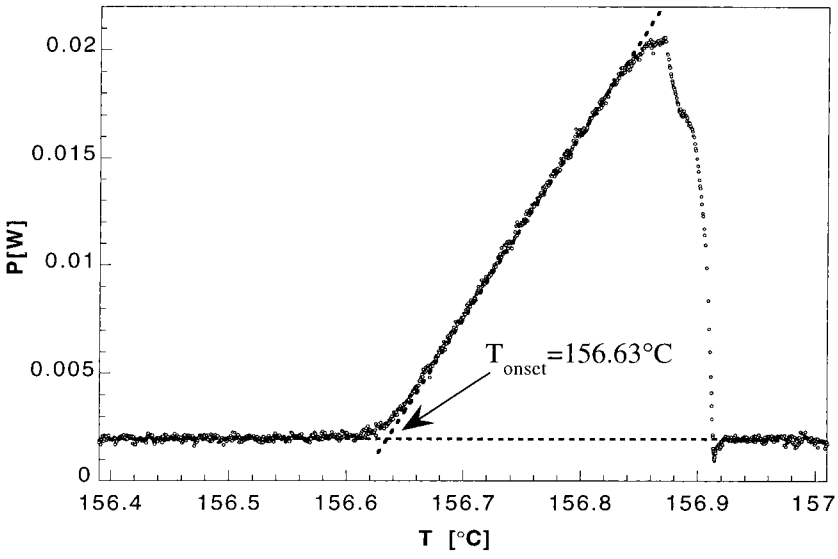

Fig. 3. Melting of indium observed in the temperature scanning mode: power supplied to the cell vs. temperature at $dT/dt = 1$ K/h. The shoulder on the high temperature side of the peak and the small exothermic signal at the end of the peak are due to the recovery time (about 50 s) of the power control unit of MASC.

scan the cell temperature at a rate of 1 K/h. The data points of the adiabatic-like step-scanning curve represent the equilibrium values of the cell temperature after each heat pulse. The apparent T_{onset} shifts upwards in the curves obtained by scanning the temperature or enthalpy. Moreover, the melting curve is stretched more and more when the scanning rate (or equivalently the supplied power) is increased, particularly near the melting end, where the relaxation time increases (Fig. 5). These effects are also significant at

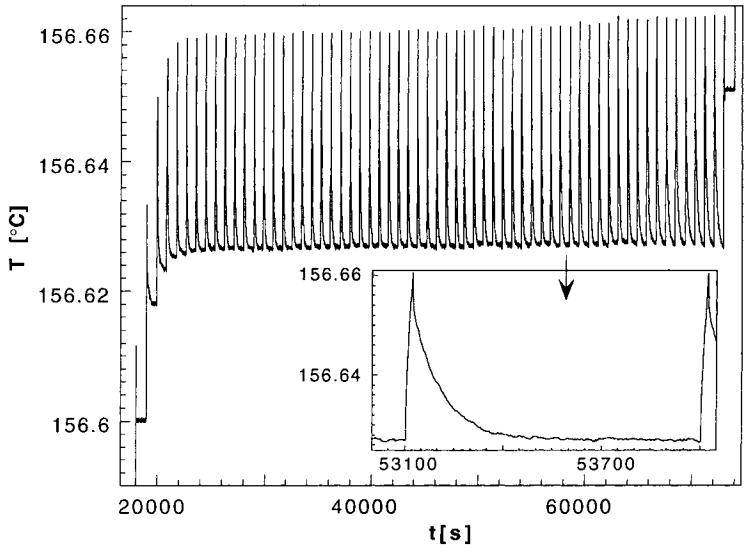

Fig. 4. Melting of indium observed in the adiabatic-like step-scanning mode: cell temperature vs. time, while supplying heat pulses of 0.25 J supplied in a period of 25 s at time intervals of 900 s. The insert shows the temperature relaxation after a heat pulse.

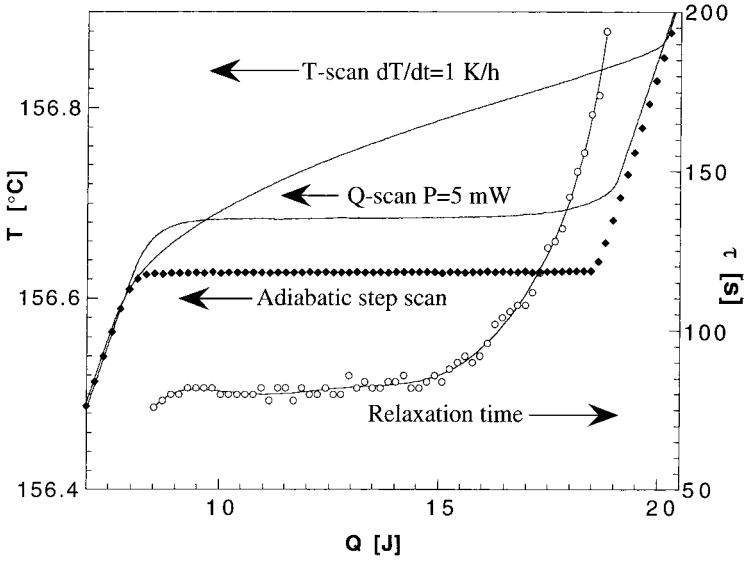

Fig. 5. Melting of indium observed in different calorimetric modes: cell temperature and cell temperature relaxation time vs. the energy supplied to the cell. The relaxation time was calculated from the temperature profile after each pulse of the adiabatic-like step-scanning run in Fig. 4.

very slow scanning rates and are due to the heat diffusion in the system and to the measuring time scale. Consequently the ''true'' melting temperature of indium is 156.626°C, i.e. the temperature measured during the adiabatic-like run in Fig. 5, which is in good agreement with the value reported in the literature (156.60°C). The melting interval is 0.0012°C, a value so small that it can be attributed either to a residual temperature gradient on the sample or to an inherent property of indium melting. The temperature relaxation time in the melting interval, due to the high thermal conductivity and the rapid melting rate of indium, represents the smallest time τ_0 which it is possible to observe with the MASC. This time is the sum of the instrumental time to transfer the heat to the sample and the heat diffusion time in the sample during melting.

4.2. Ice melting

The melting of an ice sample (from bi-distilled water) weighing 74.80 mg was studied with the MASC operating in the *T*-scanning mode at a rate of 6 K/h. The power supplied to the cell versus the cell temperature is shown in Fig. 6 and the value of T_{onset} has been derived from the graph. An adiabatic-like run, in which equal heat pulses of 0.5 J supplied in 50 s to the cell at time intervals of 900 s, is shown in Fig. 7. The graphical analysis was used to derive T_{onset} and the melting interval. The two values are −0.004 and 0.008°C, respectively. To check that the measured melting interval was not due to an artefact related to a temperature gradient on the cell, a second run was performed on a sample weighing 256 mg, i.e. about three times longer than the first one. The same result was obtained.

The melting curves of ice measured using different calorimetric modes are shown in Fig. 8. The T_{onset} value from Fig. 6 is in good agreement with the value obtained using the adiabatic-like mode. The cell temperature relaxation time of water is lower in the first part of the melting interval than that of indium, but increases to higher values towards the end of melting (compare Figs. 5 and 8). The different sample lengths and thermal conductivities of the two materials explain this behaviour. Indeed, the relaxation time of water, after correction for sample length and conductivity effects, turns out to be practically the same as τ_0 [6].

Ice exhibits a well-known pre-melting process, which is a result of the polycrystallinity and degree of impurity of the ice [15,16]. The pre-melting process

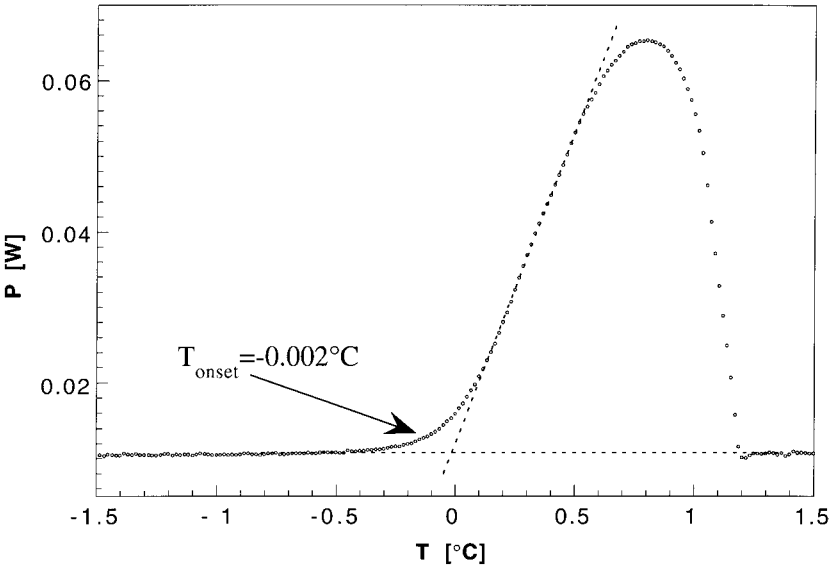

Fig. 6. Melting of ice observed in the temperature scanning mode: power supplied to the cell vs. temperature at $dT/dt = 6$ K/h.

in Fig. 6 occurs in the region just before the linear increase in the P versus T peak. In Fig. 7 its appearance is marked by an extra contribution to the enthalpy change and it ends at the beginning of the melting interval.

Important insights into the pre-melting features of ice can be obtained with modulated calorimetry, which provides direct data on the ability of the phase transition to follow the temperature modulation. The real and imaginary parts of the complex heat capacity of the water sample, measured in the power-modulated enthalpy-scanning mode, and a plot of the average cell temperature versus Q, are both shown in Fig. 9. The power supplied to the cell under adiabatic-like

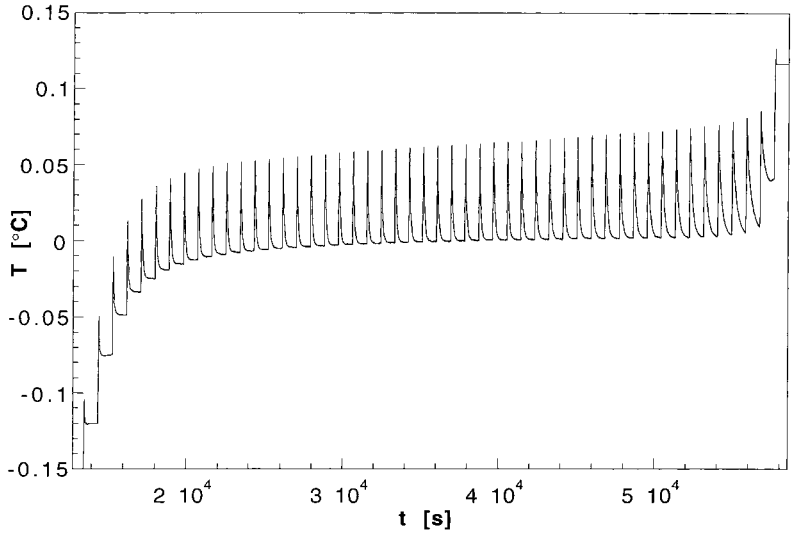

Fig. 7. Melting of ice observed in the adiabatic-like step-scanning mode: cell temperature vs. time, while supplying heat pulses of 0.25 J supplied in a period of 25 s at time intervals of 900 s.

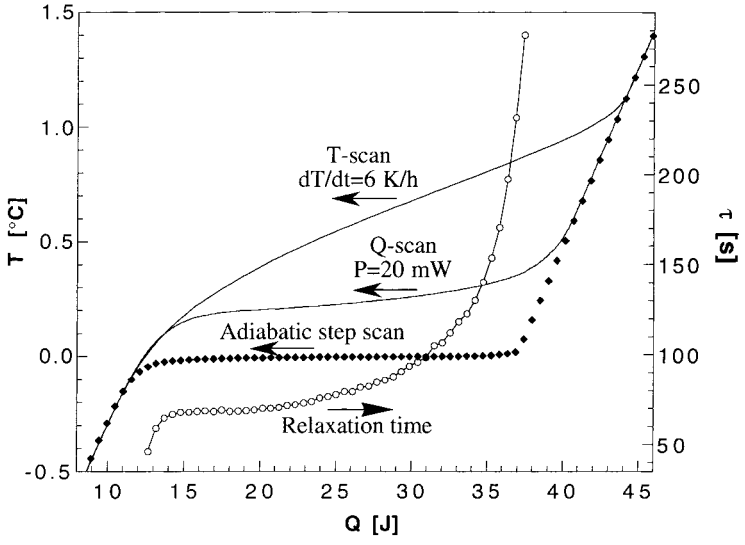

Fig. 8. Melting of ice observed in different calorimetric modes: cell temperature and cell temperature relaxation time vs. the energy supplied to the cell. The relaxation time was calculated from the temperature profile after each pulse of the adiabatic-like step-scanning run in Fig. 7.

conditions is $P(t) = P_0 + \delta P \sin(\omega t)$, where: $P_0 = 1$ mW; $\delta P = 6$ mW; $\tau = 2\pi/\omega = 600$ s. The equations used to calculate the values in Fig. 9 are reported and discussed elsewhere [5,6]. This calorimetric mode of the MASC is more appropriate than temperature-modulation to study sharp phase transitions in the frequency domain. Indeed, it is experimentally impossible to impose temperature modulation with amplitudes compatible with the transition interval. Consequently the advantages of modulated calorimetry cannot be obtained, as recently pointed out by B. Wunderlich et al. [17,18].

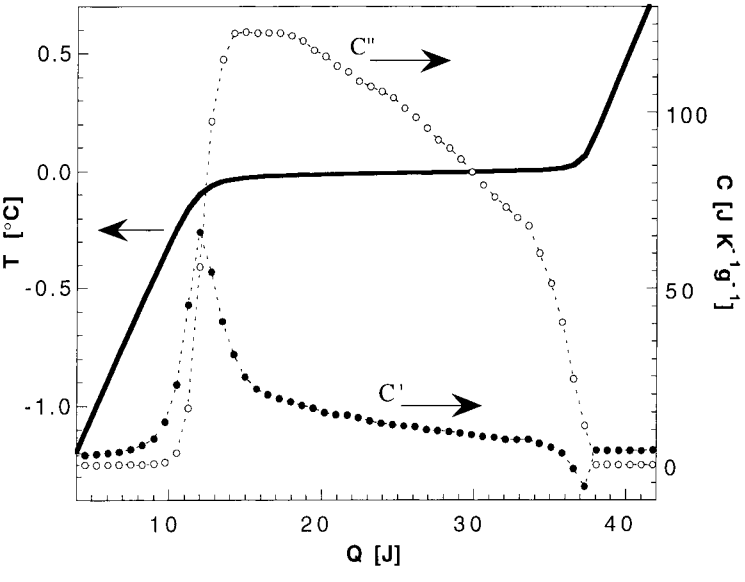

Fig. 9. Melting of ice observed in the *P*-modulated enthalpy scanning mode: the mean cell temperature and C' and C'' of the sample vs. the energy supplied to the cell. The applied power profile was $P(t) = P_0 + \delta P \sin(\omega t)$, where: $P_0 = 1$ mW; $\delta P = 6$ mW; $\tau = 2\pi/\omega = 600$ s.

4.3. Polymerisation and glass transition

The glass transition of a thermosetting polymer, observed either during the isothermal growth of the macromolecule in the chemical reaction, or scanning up/down the temperature gradient, has been thoroughly studied earlier using a differential calorimeter [5] and the results have been published [19]. The measurements carried out on a thermosetting polymer sample using the MASC showed a comparable accuracy and similar features to the previous data and so are not reported here.

In Fig. 10 the glass transition curves of polystyrene obtained using the temperature modulated scanning mode at modulation periods and modulation amplitudes in the range of 150–2400 s and 0.25–1°C, respectively, are shown. The scanning rate was 0.125 K/period. Fig. 10B shows the phase angle shift calculated from the $P(t)$ curves, measured at the reported modulation periods. The phase angle shows a broad peak from which it is possible to obtain, at least qualitatively, the glass transition temperature at the modulation frequency used. It is also possible to calculate the real and imaginary parts of the complex heat capacity and to obtain information on the glass transition [5,6]. The C' and C'' against T curves from the 600 s run are shown in Fig. 10A. The glass transition temperature is marked by the inflexion point

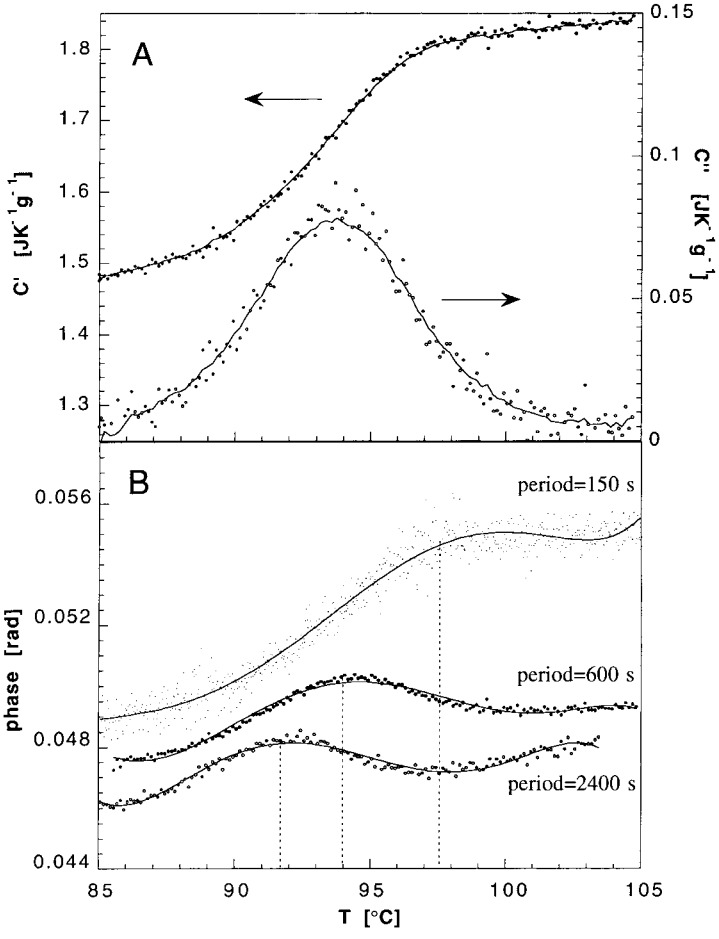

Fig. 10. Glass transition of polystyrene observed in the temperature modulated scanning mode: A, C' and C'' vs. temperature during a 600 s modulation period; B, $P(t)$ phase angle shift vs. T for different modulation periods.

of the C' curve, which is coincident with the peak of the C'' curve, as is to be expected for a dynamic transition [20].

There is general agreement regarding the advantages of modulated calorimetry for the characterisation of glassy materials. Particularly significant is the possibility of measuring vitrification simultaneously with the extent of polymerisation at the point where the transition occurs in thermosetting polymers [19].

5. Conclusions

The calorimeter described here is capable of conducting both time domain and frequency domain calorimetry on one and the same sample. The MASC can therefore be utilised for quantitative modulated calorimetry and applied to the study of phase transitions much more easily than commercially available calorimeters. Adiabatic-like calorimetry can be carried out, with all of the accompanying advantages of this operation mode, i.e. the accurate determination of the transition temperature and transition interval; increased sensitivity for studying slow processes; and better results in sample purity tests based on the melting-point depression [13]. The MASC features allow to develop a theoretical model of the cell + sample system for the analysis of the experimental data. The sample characterisation is improved by the use of combined time domain and frequency domain experiments [6].

In comparison to the two-cell differential calorimeter built earlier in the same laboratory [5], the MASC presents many significant advantages: (i) since it is a single cell calorimeter, it is easier to construct, particularly when a large sample must be studied [21]; (ii) it constitutes a multi-mode calorimeter; and (iii) its cell does not contains mercury, which not only presents a hazard in itself, but also can create problems in terms of the repeatability of successive runs on different samples. Indeed, with the earlier calorimeter it was practically impossible to avoid the adhesion of small quantities of mercury to the surface of the sample container.

The study of indium melting in the different operational modes of MASC confirms the usefulness of this element for calorimeter calibration: (i) the melting transition is practically ideal and can be utilised to test the temperature gradient in the sample cell, since the melting interval of indium is only 0.0012°C; and (ii) the temperature relaxation time (τ_0) measured in the melting interval of indium represents the time necessary to supply the latent heat of a sharp and very rapid phase transition to a sample of high thermal conductivity. Only phase transition kinetics with characteristic time longer than τ_0 could be studied.

The melting of ice occurs in a temperature interval of 0.008 ± 0.001°C. This interval is significantly larger than that of the instrument's sensitivity, also taking the apparent melting interval of indium as the limit value. The same value of the melting interval was obtained with two ice samples of different lengths (70 and 20 mm, respectively), thus excluding the effects of a temperature gradient on the cell. Below and above the melting interval of ice, modulated calorimetry gives, as do other calorimetric modes, the thermodynamic heat capacity of the solid and liquid phases, respectively. The pre-melting region is marked by an increase in C', which peaks just before the beginning of the melting interval (Fig. 9). On the contrary C'' remains practically null until a sharp increase occurs near the C' curve peak. It is evident that in the first part of the pre-melting region the cell temperature oscillates in phase with the enthalpy (the temperature relaxation time is negligible compared with the modulation period). A more detailed analysis and interpretation of the modulated calorimetry data in the melting interval would require a model for the heat diffusion in the cell + sample system, which lies beyond the scope of the present paper. However, the power-modulated enthalpy scan utilised for the study of ice melting could potentially broaden the fields of application of modulated calorimetry to the study of any type of phase transition, independently of the transition interval width.

One possible explanation for the non-null melting interval of indium and ice could be the polycrystalline nature of the samples, the fact that the melting temperature is dependent on the crystallite size, and the effect of sample impurities. Further analysis of the results reported here and further experiments will be necessary to arrive at a satisfactory explanation. Nevertheless, our preliminary data underlines the potential advantages and uses of the MASC, which offers the possibility of the combined use of different calorimetric modes. It would appear to be particularly

adapted to the study of slow phase transitions, as in ageing processes and in the crystallisation of highly viscous liquids.

References

[1] W. Henninger, G.W.H. Höhne, Calorimetry — Fundamentals and Practice, Verlag Chemie, Weinhein, 1984.
[2] R. Scherrenberb, V. Mathot, A. Van Hemelrijck, Thermochim. Acta 330 (1999) 3.
[3] E. Gmelin, Thermochim. Acta 110 (1987) 183.
[4] G. Salvetti, C. Ferrari, F. Papucci, E. Tombari, Italian Patent Deposit PI98A000044 (1998) and PI98A000073 (1998).
[5] C. Ferrari, G. Salvetti, E. Tombari, Thermochim. Acta 316 (1998) 47.
[6] E. Tombari, G. Salvetti, Theoretical model of a long cylindrical cell for multi-mode calorimetry, Thermochim. Acta, to be submitted.
[7] C. Schick, G.W.H. Höhne (Eds.), Temperature Modulated Calorimetry (special issue), Thermochim. Acta 304/305 (1997).
[8] I. Hatta, Thermochim. Acta 300 (1997) 7.
[9] G.W.H. Höhne, Thermochim. Acta 330 (1999) 45.
[10] A. Toda, T. Oda, M. Hikosaka, Y. Saruyama, Thermochim. Acta 293 (1997) 46.
[11] T. Ozawa, K. Kanari, J. Therm. Anal. 54 (1998) 521.
[12] Y.-H. Jeong, Thermochim. Acta 304/305 (1997) 67.
[13] E.E. Marti, Thermochim. Acta 5 (1972) 173.
[14] B. Wunderlich, Thermal Analysis, Academic Press, Boston, 1990.
[15] G.P. Johari, W. Pascheto, S.J. Jones, J. Chem. Phys. 100 (1994) 4548.
[16] G. Salvetti, E. Tombari, G.P. Johari, J. Chem. Phys. 102 (1995) 4987.
[17] A. Boller, M. Ribeiro, B. Wunderlich, J. Therm. Anal. 54 (1998) 545.
[18] B. Wunderlich et al., Thermochim. Acta 330 (1999) 21.
[19] C. Ferrari, G. Salvetti, E. Tombari, G.P. Johari, Phys. Rev. E 54 (1996) 1058.
[20] C.J.F. Bottcher, P. Bodewijk, Theory of Dielectric Polarization, Vol. II, 2nd Edition, Elsevier, Amsterdam, 1978 (Chapter 8).
[21] E. Tombari, C. Ferrari, G. Salvetti, Chem. Phys. Lett. 300 (1999) 749.